BOLETIN DE LA SOCIEDAD ESPAÑOLA DE
Cerámica y Vidrio
www.elsevier.es/bsecv

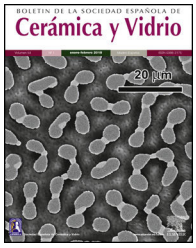

Production of Al_2O_3–SiC nano-composites by spark plasma sintering

*Mansour Razavi**, *Ali Reza Farajipour*, *Mohammad Zakeri*, *Mohammad Reza Rahimipour*, *Ali Reza Firouzbakht*

Department of Ceramic, Materials and Energy Research Center (MERC), P.O. Box 14155-4777, Tehran, Iran

ARTICLE INFO

Article history:
Received 19 November 2016
Accepted 24 January 2017
Available online 20 February 2017

Keywords:
Sintering
Hardness
Nano-composite
SPS
Strength
Density
XRD
Wear

ABSTRACT

In this paper, Al_2O_3–SiC composites were produced by SPS at temperatures of 1600 °C for 10 min under vacuum atmosphere. For preparing samples, Al_2O_3 with the second phase including of micro and nano-sized SiC powder were milled for 5 h. The milled powders were sintered in a SPS machine. After sintering process, phase studies, densification and mechanical properties of Al_2O_3–SiC composites were examined. Results showed that the specimens containing micro-sized SiC have an important effect on bulk density, hardness and strength. The highest relative density, hardness and strength were 99.7%, 324.6 HV and 2329 MPa, respectively, in Al_2O_3–20 wt% SiC_{micro} composite. Due to short time sintering, the growth was limited and grains still remained in nano-meter scale.

Producción de nano-composites – SiC–Al_2O_3 por spark plasma sinterizado

Palabras clave:
Sinterización
Dureza
Nano-composite
SPS
Fuerza
Densidad
DRX
Desgaste

RESUMEN

En este trabajo se muestran compuestos de Al_2O_3-SiC producidos por SPS, en vacío, a 1.600 °C durante 10 min. Para la preparación de muestras, se molieron polvos de Al_2O_3 durante 5 h con la segunda fase de micro-y-nano polvo de SiC. Posteriormente, estos polvos molidos se sinterizaron mediante SPS. Después del proceso de sinterización, se realizaron estudios de fase, densificación y propiedades mecánicas de los compuestos de Al_2O_3-SiC obtenidos. Los resultados mostraron que micro-SiC en las muestras tiene un efecto importante en su densidad aparente, dureza y resistencia. La mayor densidad relativa, dureza y resistencia fueron respectivamente del 99,7%, 324,6 HV y 2.329 MPa para Al_2O_3 con un 20% en peso micro-SiC. Debido al corto tiempo de sinterización, el crecimiento los granos fue limitado y se mantuvieron en escala nanométrica.

* *Corresponding author.*
E-mail address: m-razavi@merc.ac.ir (M. Razavi).
http://dx.doi.org/10.1016/j.bsecv.2017.01.002

Introduction

Thermal and chemical stability, relatively high strength, thermal and electrical insulator alongside the availability and abundance of aluminum oxide, lead to use of this material in engineering applications [1–5]. Despite the mentioned advantages, low fracture toughness of this material lead to limitation of its application. Composites are one of the methods which over come to this limitation. In this technique alumina matrix is reinforced by particles or fibers as secondary phase, which can be metal, polymer or ceramic. Silicon carbide (SiC) as a ceramic material can be one of the option which leads to improvement of alumina matrix [6–10]. Nihara et al. reported that sintering of Al_2O_3–SiC composite was done successfully. They found out that adding a little amount of SiC to alumina matrix can improve mechanical properties of composite significantly in comparison with non-composite materials. They increased strength and fracture toughness from 350 to 1520 MPa and 3.5 to 4.8 $MPam^{1/2}$, respectively by adding 5 vol.% SiC [11].

There are different methods of sinter this composite. Non-pressure and hot press sintering are the most common method of sintering for this composite, but new technique which is considerable today is spark plasma sintering (SPS) [6,12–15]. On the base of spark plasma, which is created by a pulsed direct current, SPS leads to quick increasing of mold's and the powder's temperature. High heating rate, using pressure and electrical current is the specifications of this technique which distinguish this technique in comparison with other method. In addition to reduction of particle's coarsening, high heating rate increased condensation through the elimination of surface diffusion mechanism and creating of extra driving force by high temperature gradient. Pressure applying during the heating can increase the driving force of process and facilitate the sintering process. Electrical current can condense the powder in mold by creating of many sparks between particles and creating of plasma environment. Effect of plasma on surface's cleanness of particles and improvement of sintering process has been reported by researchers [16–21].

Synthesis of Al_2O_3–SiC composite by SPS has been investigated by a few researchers [16,17], but the effect of particle size on the densification, mechanical and wear properties has not been reported until now. So in this paper sintering process and properties of Al_2O_3 matrix reinforced by micro and nano-sized SiC will be examined.

Experimental

Al_2O_3 and SiC powders in micro and nano-meter scale with purity 99.8%, 99.5% and 99.9% and mean particle size of 1.5 μm, 10 μm and 50 nm, respectively were used as raw materials. Al_2O_3 powder with two sources of SiC (micro and nano as systems 1 and 2, respectively) powder were milled in a planetary ball mill (as a high energy ball mill) for 5 h in distilled water. Ball to powder ratio was 10 to 1 in all tests. In the following, prepared powders were sintered in a mold with 8 cm in diameter under specific conditions according to Table 1 by SPS

Table 1 – Coding and sintering conditions of samples.

System* SiC	Code of sample	Composition (wt.%)			Diameter of mold (mm)	Maximum temperature (°C)	Maximum pressure (MPa)	Soaking time (min)	Milling time (min)
		Al_2O_3	SiC (micrometer)	SiC (nanometer)					
–	A	100	–	–	8	1600	20	10	–
	5m	95	5	–	8	1600	20	10	300
	10m	90	10	–	8	1600	20	10	300
1 (Micro)	15m	85	15	–	8	1600	20	10	300
	20m	80	20	–	8	1600	20	10	300
	5n	95	–	5	8	1600	20	10	300
2 (Nano)	10n	90	–	10	8	1600	20	10	300

* Systems 1 and 2 are composites with the second phase including of micro and nano-sized SiC, respectively.

machine. The sintering process was done under high pulsed direct current (1000–3500 A) in vacuum. A uniaxial pressure of 10 MPa was used during the reaction and increased to 20 MPa after reaching to the expected temperature and maintained during holding time. After holding time the uniaxial pressure decreased to 10 MPa and maintained during cooling.

After sintering process, the samples were polished and cut. In order to detect of phases in sample's structure and evaluate of properties XRD (Siemens, 30 kV, 25 mA, Cu Kα) was used. The crystallite size and strain were evaluated through Scherrer and Williamson–Hall methods applying the following equations [18]:

$$d = \frac{0.9\lambda}{b\cos\theta} \quad \text{Scherrer equation}$$

$$B\cos\theta = \frac{0.9\lambda}{d} + 2\eta\sin\theta \quad \text{Williamson-Hall equation}$$

where B, θ, λ, d and η are the full width of the peak at half intensity (rad.), position of peak in the pattern (rad.), the wavelength of X-ray (nm), crystalline size (nm), and mean internal strain, respectively.

Samples density, open and closed porosity and water absorption were estimated by Archimedes method [19]. Strength of the samples was measured through three points test. Five samples with dimension of $3 \times 4 \times 45$ mm were prepared and average of strength reported [20]. Hardness of the sample was determined through Vickers method. 5 tests were done for each sample and average of results were reported [21]. Microstructures of milled and sintered samples were studied by scanning electron microscope (Cambridge model). Finally, wear resistance of samples was done in order to determine the wear properties. In this test composite samples were used as a pin and alumina was used as the disc. The force on the pin tip was 15.3 N. The machine was stopped in the distances of 1000 m and the weight losses of the samples were with the accuracy of 0.0001 g [22].

Result and discussion

Patterns of X-ray diffraction of milled powders are illustrated in Fig. 1. As it is seen in these patterns, milling has not led to phase transfer in raw materials, and identified phases are Al_2O_3 and SiC with 1125-071-01 and 00-002-1048 reference code, respectively. As it stands, by increasing of SiC phase, intensity of their peaks has been increased. Crystalline size (d) and mean strain (η) of milled powder were measured. The changes of $B{\cdot}\cos\theta$ to $2\sin\theta$ are seen in Fig. 2. Calculation results are brought in Table 2, as it is seen in this table crystalline size of milled powder in all compounds for both phases are in nano-meter scale. The crystalline sizes of milled samples (which all of them have been treated in a similar way) have a range between 36 and 40 nm and 17 and 36 nm for Al_2O_3 and SiC phases, respectively and no significant difference between sizes. As it stands, size of phases in the second system is finer than first system, that can be attributed to two reasons: the first one is using of SiC with nano scale in the second system and the next one is the presence of more finer SiC particles in the second system at equal weight fraction which can operate as fine balls and facilitate of milling process. These particles increases milling energy and lead to crush of particles [23].

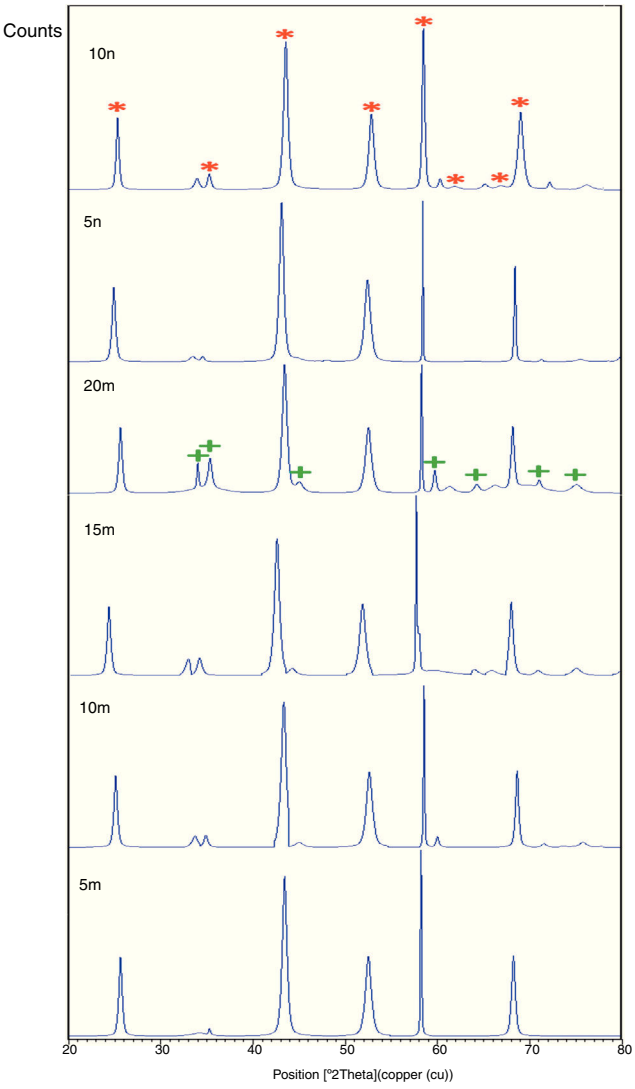

Fig. 1 – X-ray patterns of milled samples (*) Al_2O_3, (+) SiC.

SEM image form milled samples are presented in Fig. 3. As it is obvious in this figure, milling lead to decreasing the size of particles in both systems and the mean particle sizes are in nanometer scale. The size of particles in the system containing nano SiC are lower than the system without that.

X-ray pattern of sintered sample is brought in Fig. 4, as it is seen, there is no change in phases of sintered samples and in milled sample (Fig. 1), Al_2O_3 and SiC are identified phases. As it is obvious in Fig. 5, the only considerable point in comparison of this pattern with milled sample pattern is increasing of peak's intensity and decreasing of peak's width in sintered sample. Increasing of temperature during the sintering can lead to growth of crystals and reducing of mean lattice strain [24,25].

The changes of $B{\cdot}\cos\theta$ to $2\sin\theta$ in sintered samples are shown in Fig. 6. The results of these calculations are brought in Table 2. As these calculations show, although the crystalline sizes are in nanometer scale with the range of 59–66 nm and 30–52 nm for Al_2O_3 and SiC phases, respectively but sintering leads to growth of crystals and decreasing of mean

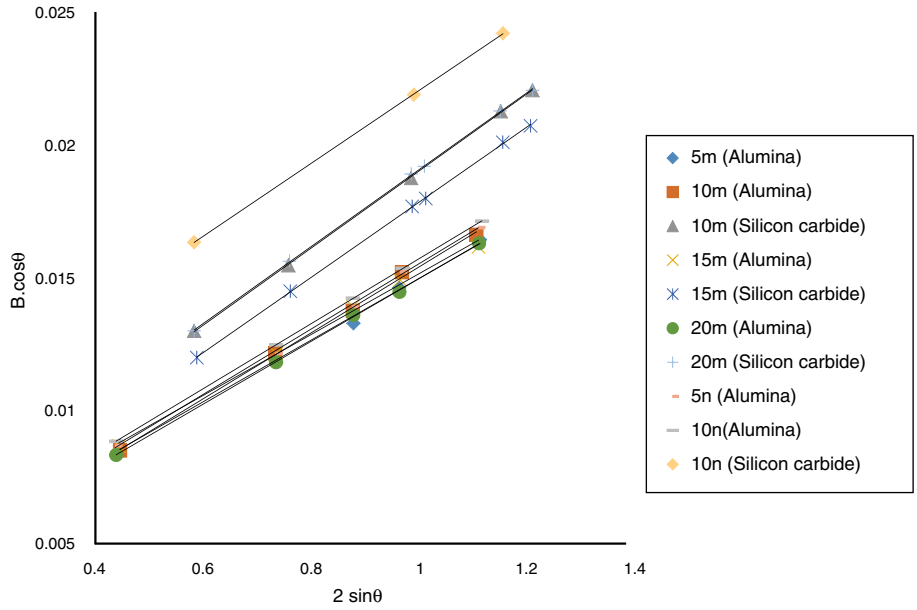

Fig. 2 – W–H diagram of milled samples for calculation of crystalline sizes and mean strains of phases.

lattice strain slightly. Unlike common methods of sintering, which follow extreme growth, sintering though SPS has a little growth, so that the crystals are in nano scale yet. When the sintering (including heating and keeping processes) is completed in a few minutes, the crystals could be small [26].

The changes of sample's thickness to time for sample which contain different amount of SiC include three zones. At first, the time of less than 35 min, which sample has been heated and has a little expansion. In the following by increasing the temperature, sintering process occurred and samples were contracted quickly during about 5 min and then change of displacement will be constant. As it stands, the sintering process was completed at the end of second zone and samples were dense. According to the changes of sample thickness and temperature versus sintering time plots, beginning temperature of sintering (beginning of second zone) is determined. This information is brought in Table 3. Decrease in thickness of the samples and the starting of second zone is due to the overcoming of contraction of sintering on thermal expansion of the samples.

Table 2 – Results of calculations of crystalline sizes and mean strain of milled and sintered samples.

Code of sample		Phase	Crystalline size (nm)	Mean strain (%)	Used method
Milled samples	5m	Al_2O_3	40	1.14	W–H
		SiC	35	–	Scherrer
	10m	Al_2O_3	45	1.22	W–H
		SiC	30	1.43	W–H
	15m	Al_2O_3	36	1.13	W–H
		SiC	36	1.39	W–H
	20m	Al_2O_3	43	1.16	W–H
		SiC	29	1.42	W–H
	5n	Al_2O_3	42	1.21	W–H
		SiC	19	–	Scherrer
	10n	Al_2O_3	39	1.20	W–H
		SiC	17	1.35	W–H
Sintered samples	5m	Al_2O_3	61	0.97	W–H
		SiC	52	–	Scherrer
	10m	Al_2O_3	63	0.94	W–H
		SiC	52	1.10	W–H
	15m	Al_2O_3	60	1.03	W–H
		SiC	50	1.10	W–H
	20m	Al_2O_3	59	0.95	W–H
		SiC	52	1.14	W–H
	5n	Al_2O_3	65	1.01	W–H
		SiC	33	–	Scherrer
	10n	Al_2O_3	66	1.07	W–H
		SiC	30	1.02	W–H

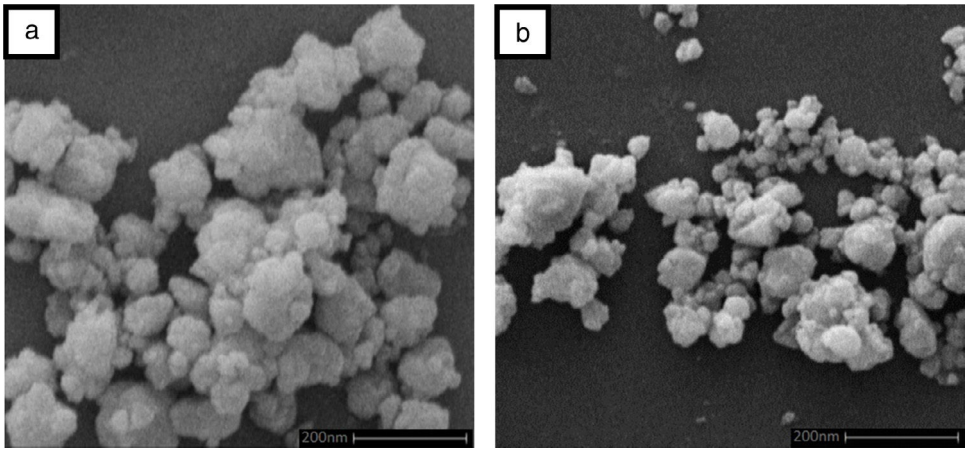

Fig. 3 – Microstructure of milled samples for 300 min (a) 10m sample and (b) 10n sample.

As it is seen in Table 3, in the first system by increasing of SiC to 10 wt.%, beginning temperature of sintering has been increased and then decreased. SiC with higher melting point than Al_2O_3, increase the sintering temperature of Al_2O_3. But increasing of SiC which has lower thermal expansion (TEC) coefficient in comparison with Al_2O_3 leads to decreasing of thermal expansion coefficient of composite (melting point and thermal expansion of Al_2O_3 and SiC are 2072 °C and 8.1×10^{-6}/°C and 2730 °C and 4.0×10^{-6}/°C, respectively) [27]. Hence the early expansion has been decreased during the heating and as a result beginning temperature of contraction is decreased too. So, after 10 m sample, decrease of sintering temperature is seen. This treatment is similarly seen in second system too. Only in this system, overcoming of the second phenomenon to first one is quicker than and is happened in less amount of SiC.

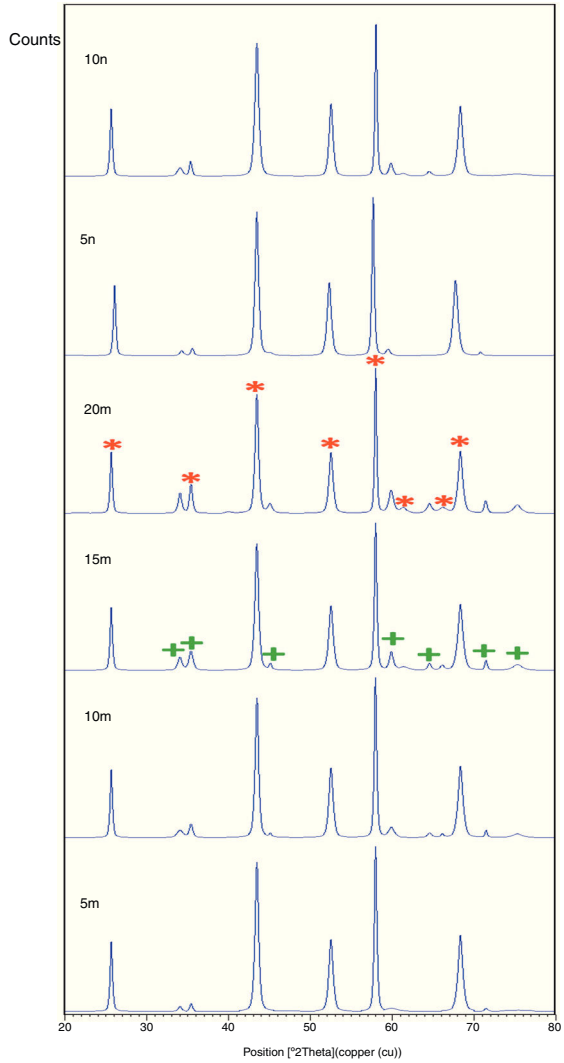

Fig. 4 – X-ray patterns of sintered samples (*) Al_2O_3, (+) SiC.

Table 3 – Temperature of sintering with physical properties of sintered samples.

Code of sample	Temperature of sintering (°C)	Relative density (%)	Amount porosity (%)	Water absorption (%)
A	1162	95.4	4.6	0.2
5m	1251	99.7	0.3	–
10m	1315	99.5	0.5	0.03
15m	1220	99.5	0.5	0.08
20m	1142	99.7	0.3	–
5n	1273	94.6	5.4	1.32
10n	1133	92	8	1.93

The changes of relative density of sintered samples for the two systems are presented in Table 3. As it is obvious, in system 1, addition of different amount of SiC to Al_2O_3 matrix leads to completing of sintering and achievement to samples with nearly full density. Lower sintering temperature, short temperature and holding times have prepare it possible to produce nano-composite of SiC–Al_2O_3 to near theoretical density with little crystal growth [28]. To attainment full density by common sintering technique, higher temperature and soaking time is needed. Shi et al. succeeded to sinter Al_2O_3–SiC composite with relative density of 100% via hot press technique at temperature over 1700 °C. They reported sintering by hot press leaded to abnormal growth in some samples [29].

Against, presence of nano-sized SiC in system 2 could not obtain a sample with high density. A great difference between particle size of matrix and the reinforcement phase in the

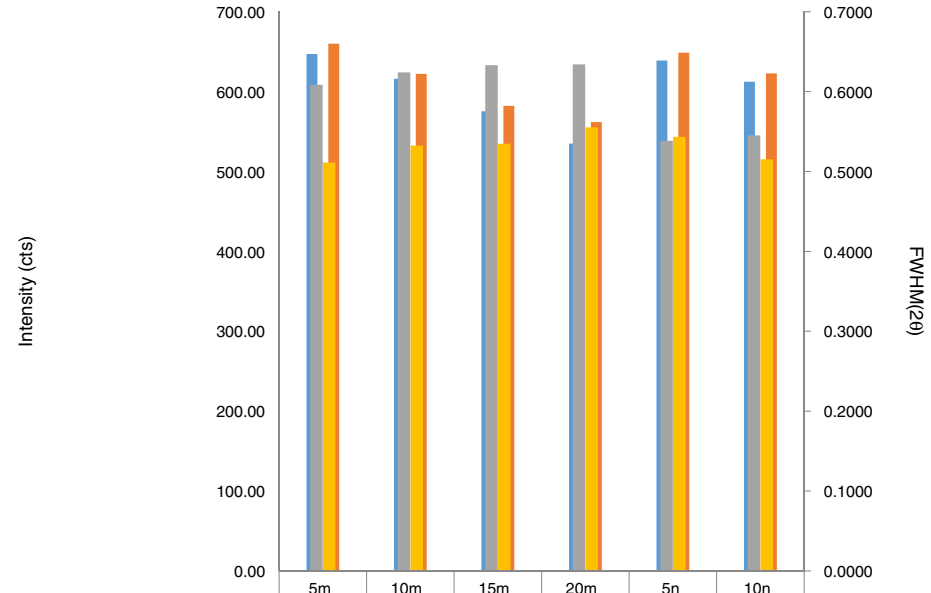

	5m	10m	15m	20m	5n	10n
Intensity after milling (cts)	647.10	616.10	575.31	534.81	638.86	612.33
Intensity after sintering (cts)	659.99	622.22	582.11	561.88	648.64	622.74
FWHM after milling (2θ)	0.6085	0.6240	0.6331	0.6341	0.5384	0.5451
FWHM after sintering (2θ)	0.5112	0.5324	0.5347	0.5552	0.5434	0.5153

Fig. 5 – The changes of intensity and full width at half maximum (FWHM) of alumina peak for milled and sintered samples ($2\theta = 40–45°$).

second system decreased packing and leads to decrease of final density. There is evidence when a SiC as fine component are added to the Al_2O_3 particles, it adhere to the large particles strongly and delay the penetration of fine components to the mixtures [30]. Wide distribution of particles in system 2 confirms this point (Fig. 3b). Furthermore, as it is obvious in Table 3, by increasing the weight percent of SiC, density is decreased. This could be due to the poor sintering property of SiC at examined temperatures in this paper. Similar result was reported by other researchers [29,31,32].

Fig. 7 shows the SEM images for the microstructure of the sintered compacts. There are two different phases in both systems, i.e., dark and light phase. As it is seen from Fig. 4 and as it was discussed earlier, XRD pattern implied that there was no reaction between the raw materials. So Al_2O_3 and SiC are only phases in sintered samples. According to these images,

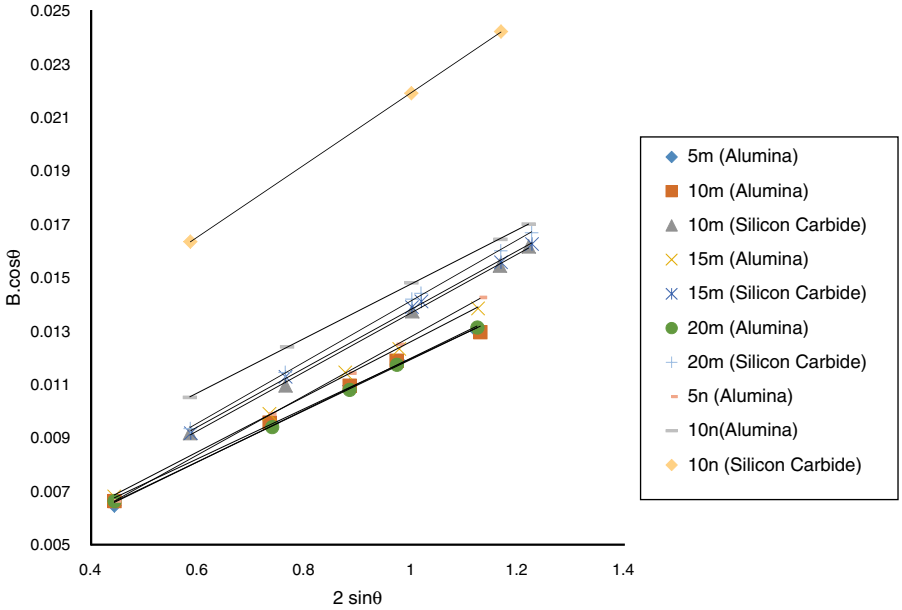

Fig. 6 – W–H diagram of sintered samples for calculation of crystalline sizes and mean strains of phases.

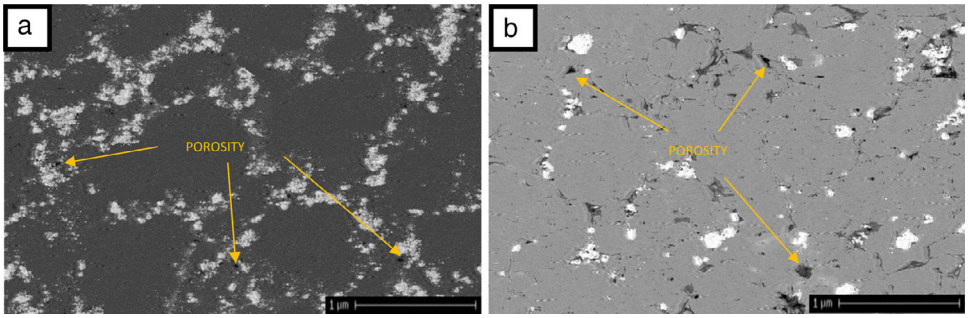

Fig. 7 – Microstructure of sintered samples (a) 10m sample and (b) 10n sample.

SiC with lower mass absorption coefficient than Al_2O_3 as light and dark phases, respectively were dispersed in the matrix [33,34]. As it was calculated porosity by Archimedes method, porosity can be seen in microstructural images of samples. The amount and sizes of porosity in system 2 is higher than system 1.

Flexural strength and hardness of sintered samples are illustrated in Fig. 8. As it stands, in system 1 with a density close to each other, the flexural strength of samples increased by increasing the amount of SiC particles up to 10% and after that adding more SiC could not increase the flexural strength. When the weight percent of SiC was more than 10, a suitable distribution of this phase cannot be seen [32,35]. Existence of hard SiC particles with a fine structure could be improve the mechanical properties [36]. Furthermore, due to residual stress from the mismatch of TEC between SiC and Al_2O_3, matrix is under the compressive stress during cooling. So, existence of SiC in the matrix of Al_2O_3 increases the strength [37]. Adding hard SiC as reinforcement phase to the Al_2O_3 matrix could increase the hardness numbers significantly (hardness of SiC and Al_2O_3 are 1175 HV and 2800 HV) [27]. Since in system 2 achievements to samples with full density were not happening, flexural strength and hardness were weaker than specimens of first system. The porosity effects on the mechanical properties of ceramic materials meaningfully [29].

Loss of weight in the sample after wear resistance is seen in Fig. 9. Due to high hardness in sample which contain hard SiC, wear resistance of them are increased. During dry sliding, the SiC particles do not easily come out in the debris because of their reasonably good bonding with the matrix. By decreasing the particle size, bonding takes place better and the wear resistance increases. Furthermore, the formation of oxide layer on the wear surface of the composite reduced wear resistance. These oxides consist of very fine with sizes of about 10–100 nm

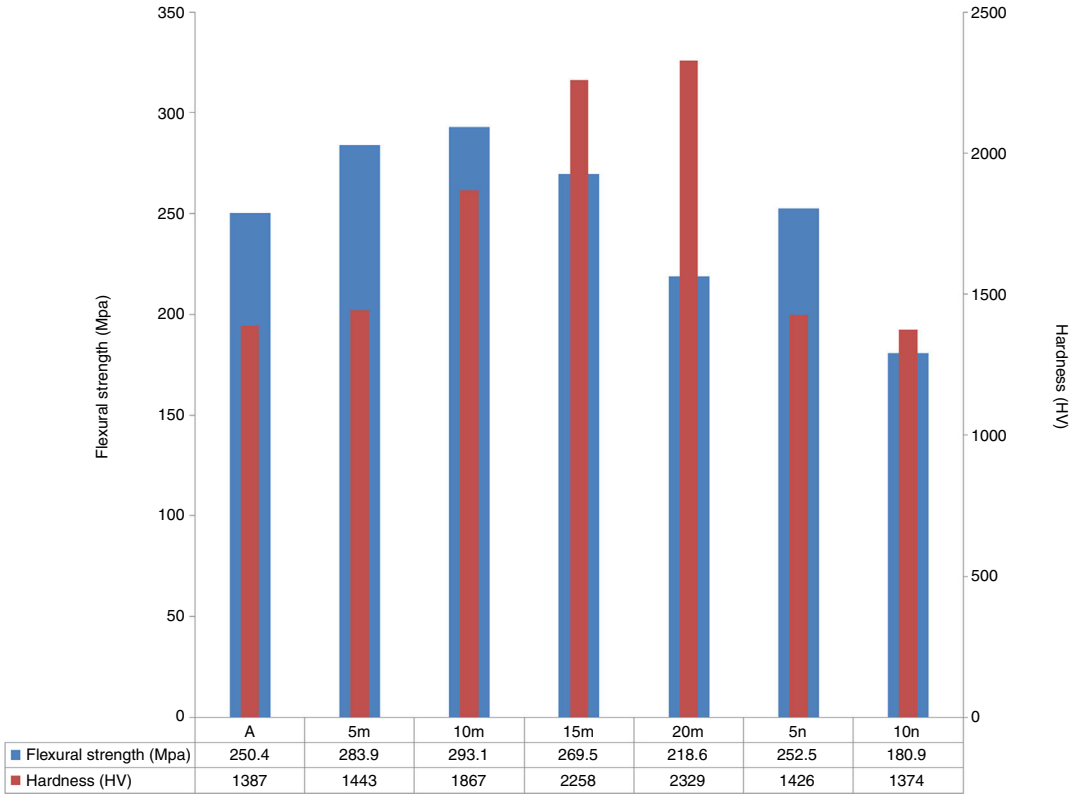

	A	5m	10m	15m	20m	5n	10n
Flexural strength (Mpa)	250.4	283.9	293.1	269.5	218.6	252.5	180.9
Hardness (HV)	1387	1443	1867	2258	2329	1426	1374

Fig. 8 – The changes of flexural strength and hardness of sintered samples.

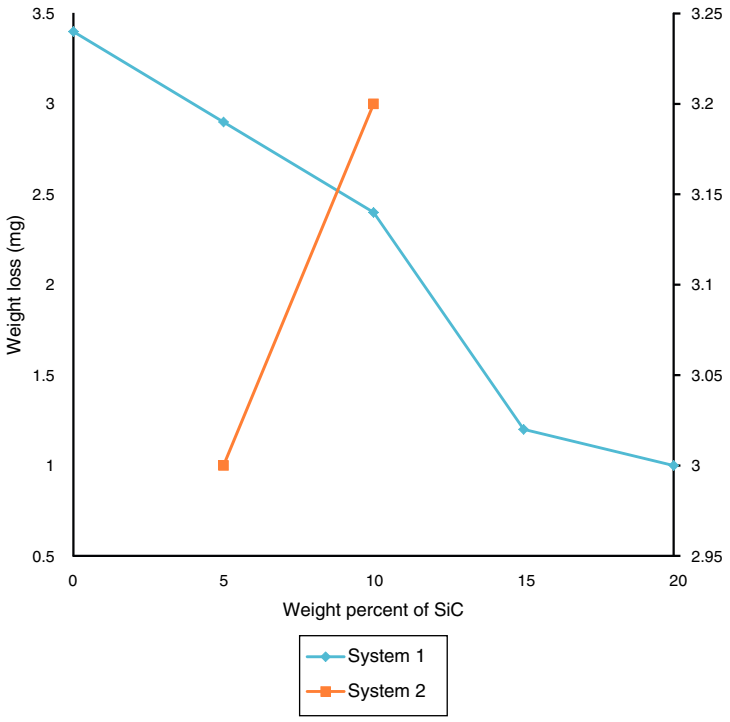

Fig. 9 – The changes of weight of sintered samples during wear test.

which have been compacted onto the composite's surface, preexisting surface oxide layers, or compressed coarse wear debris [38]. Because of lower density of samples in the second system, wear properties of these samples are lower than the first system.

Conclusion

Al_2O_3–SiC composites were prepared successfully by SPS with relative density of 100%. The composites with denser structure have higher flexural strength. 293.1 MPa and 2329 HV of the highest hardness and flexural strength were obtained from the samples reinforced by 10 and 20 wt.% SiC, respectively. By increasing the amount of SiC, flexural strength was improved first and then decreases because of a bad distribution of seconded phase in the matrix. Due to lower density in samples containing nano-sized SiC, mechanical properties were weaker than specimens of the first system.

REFERENCES

[1] R. Iglesias, M. Rivas, J.C.R. Reis, T. Iglesias, Permittivity and electric conductivity of aqueous alumina (40 nm) nanofluids at different temperatures, J. Chem. Thermodyn. 89 (2015) 189–196.
[2] R.H. Castro, On the thermodynamic stability of nanocrystalline ceramics, Mater. Lett. 96 (2013) 45–56.
[3] J. Bai, X. Yang, S. Xu, Y. Shi, J. Yang, Fabrication of highly dense Al_2O_3 ceramics, Scripta Mater. 68 (2013) 393–395.
[4] W.D. Callister, D.G. Rethwisch, Materials Science and Engineering: An Introduction, Wiley, New York, 2007.
[5] S. Yoshioka, L. Boatemaa, S. van der Zwaag, W. Nakao, W.G. Sloof, On the use of TiC as high-temperature healing particles in alumina based composites, J. Eur. Ceram. Soc. 36 (2016) 4155–4162.
[6] B. Baron, C. Kumar, G. Le Gonidec, S. Hampshire, Comparison of different alumina powders for the aqueous processing and pressureless sintering of Al_2O_3–SiC nanocomposites, J. Eur. Ceram. Soc. 22 (2002) 1543–1552.
[7] K. Niihara, A. Nakahira, T. Uchiyama, T. Hirai, High-temperature mechanical properties of Al_2O_3–SiC cmposites, in: Fracture Mechanics of Ceramics, Springer, 1986, pp. 103–116.
[8] S. Grasso, T. Saunders, H. Porwal, B. Milsom, A. Tudball, M. Reece, Flash Spark Plasma Sintering (FSPS) of α and β SiC, J. Am. Ceram. Soc. 99 (2016) 1534–1543.
[9] C. Gutiérrez-González, M. Suarez, S. Pozhidaev, S. Rivera, P. Peretyagin, W. Solís, L. Díaz, A. Fernandez, R. Torrecillas, Effect of TiC addition on the mechanical behaviour of Al_2O_3–SiC whiskers composites obtained by SPS, J. Eur. Ceram. Soc. 36 (2016) 2149–2152.
[10] P. Mohanty, S. Mohapatra, J. Mohapatra, S. Singh, P. Padhi, D. Mishra, Utilization of chemically synthesized fine powders of SiC/Al_2O_3 composites for sintering, Mater. Manuf. Process. 31 (2016) 1311–1317.
[11] K. Niihara, New design concept of structural ceramics–ceramic nanocomposites, Nippon Seramikkusu Kyokai Gakujutsu Ronbunshi 99 (1991) 974–982.
[12] I.A. Chou, H.M. Chan, M.P. Harmer, Effect of annealing environment on the crack healing and mechanical behavior of silicon carbide-reinforced alumina nanocomposites, J. Am. Ceram. Soc. 81 (1998) 1203–1208.
[13] D. Sciti, J. Vicens, A. Bellosi, Microstructure and properties of alumina-SiC nanocomposites prepared from ultrafine powders, J. Mater. Sci. 37 (2002) 3747–3758.
[14] I. Ahmad, M. Islam, T. Subhani, Y. Zhu, Toughness enhancement in graphene nanoplatelet/SiC reinforced Al_2O_3

ceramic hybrid nanocomposites, Nanotechnology 27 (2016) 425704.
[15] R. Aroshas, I. Rosenthal, A. Stern, Z. Shmul, S. Kalabukhov, N. Frage, Silicon carbide diffusion bonding by spark plasma sintering, Mater. Manuf. Process. 30 (2015) 122–126.
[16] J.H. Chae, K.H. Kim, Y.H. Choa, J.-i. Matsushita, J.-W. Yoon, K.B. Shim, Microstructural evolution of Al_2O_3–SiC nanocomposites during spark plasma sintering, J. Alloy Compd. 413 (2006) 259–264.
[17] G. Raju, B. Basu, Spark plasma sintering of nanoceramic composites, Compr. Hard Mater. 2 (2014) 177–205.
[18] M. Razavi, M.R. Rahimipour, R. Mansoori, Synthesis of TiC–Al_2O_3 nanocomposite powder from impure Ti chips, Al and carbon black by mechanical alloying, J. Alloy Compd. 450 (2008) 463–467.
[19] ASTM, B962, Standard Test Methods for Density of Compacted or Sintered Powder Metallurgy (PM) Products Using Archimedes' Principle, ASTM, International, West Conshohocken, PA, USA, 2011.
[20] ASTM, C1161, Standard Test Method for Flexural Strength of Advanced Ceramics at Ambient Temperature, ASTM, International, West Conshohocken, PA, USA, 2011.
[21] ASTM, E384, Standard Test Method for Knoop and Vickers Hardness of Materials, ASTM, International, West Conshohocken, PA, USA, 2011.
[22] ASTM, G99, Standard Test Method for Wear Testing with a Pin-on-Disk Apparatus, ASTM, International, West Conshohocken, PA, USA, 2008.
[23] M. Razavi, M.R. Rahimipour, R. Yazdani-Rad, A novel technique for production of nano-crystalline mono tungsten carbide single phase via mechanical alloying, J. Alloy Compd. 509 (2011) 6683–6688.
[24] M. Razavi, A.H. Rajabi-Zamani, M.R. Rahimipour, R. Kaboli, M.O. Shabani, R. Yazdani-Rad, Synthesis of Fe–TiC–Al_2O_3 hybrid nanocomposite via carbothermal reduction enhanced by mechanical activation, Ceram. Int. 37 (2011) 443–449.
[25] M. Razavi, M.R. Rahimipour, Effect of mechanical activation on syntheses temperature of TiC reinforced iron-based nano-composite from ilmenite concentrate, Ceram. Int. 35 (2009) 3529–3532.
[26] M. Omori, Sintering, consolidation, reaction and crystal growth by the spark plasma system (SPS), Mater. Sci. Eng. A 287 (2000) 183–188.
[27] W.G. Fahrenholtz, E.J. Wuchina, W.E. Lee, Y. Zhou, Ultra-high Temperature Ceramics: Materials for Extreme Environment Applications, John Wiley & Sons, 2014.
[28] Z. Munir, U. Anselmi-Tamburini, M. Ohyanagi, The effect of electric field and pressure on the synthesis and consolidation of materials: a review of the spark plasma sintering method, J. Mater. Sci. 41 (2006) 763–777.
[29] X. Shi, F. Xu, Z. Zhang, Y. Dong, Y. Tan, L. Wang, J. Yang, Mechanical properties of hot-pressed Al_2O_3/SiC composites, Mater. Sci. Eng. A 527 (2010) 4646–4649.
[30] E. Abdullah, D. Geldart, The use of bulk density measurements as flowability indicators, Powder Technol. 102 (1999) 151–165.
[31] A.R. Moradkhani, H.R. Baharvandi, A. Vafaeesefat, M. Tajdari, Microstructure and mechanical properties of Al_2O_3–SiC nanocomposites with 0.05% MgO and different SiC volume fraction, Int. J. Adv. Design Manuf. Technol. 5 (2012) 99.
[32] A.R. Yazdi, H. Baharvandi, H. Abdizadeh, J. Purasad, A. Fathi, H. Ahmadi, Effect of sintering temperature and siliconcarbide fraction on density, mechanical properties and fracture mode of alumina–silicon carbide micro/nanocomposites, Mater. Design 37 (2012) 251–255.
[33] J. Goldstein, D.E. Newbury, P. Echlin, D.C. Joy, A.D. Romig Jr., C.E. Lyman, C. Fiori, E. Lifshin, Scanning Electron Microscopy and X-ray Microanalysis: A Text for Biologists, Materials Scientists, and Geologists, Springer Science & Business Media, 2012.
[34] D.C. Joy, A.D. Romig Jr., Principles of Analytical Electron Microscopy, Springer Science & Business Media, 1986.
[35] S. Meguid, Y. Sun, On the tensile and shear strength of nano-reinforced composite interfaces, Mater. Design 25 (2004) 289–296.
[36] D.W. Bäuerle, Laser Processing and Chemistry, Springer Science & Business Media, 2013.
[37] J. Luo, R. Stevens, The role of residual stress on the mechanical properties of Al_2O_3–5 vol% SiC nano-composites, J. Eur. Ceram. Soc. 17 (1997) 1565–1572.
[38] M. Farrokhzad, T. Khan, Sliding wear performance of nickel-based cermet coatings composed of WC and Al_2O_3 nanosized particles, Surf. Coat. Technol. 304 (2016) 401–412.